Journal of Solid State Chemistry 181 (2008) 3287–3293

Contents lists available at ScienceDirect

Journal of Solid State Chemistry

journal homepage: www.elsevier.com/locate/jssc

Predicted energies and structures associated with the mixed calcium strontium fluorapatites

Emily M. Michie [a], Robin W. Grimes [a,*], Shirley K. Fong [b], Brian L. Metcalfe [b]

[a] Department of Materials, Imperial College London, London SW7 2AZ, UK
[b] Materials Science Research Division, AWE, Aldermaston, Berkshire, RG7 4PR, UK

ARTICLE INFO

Article history:
Received 13 May 2008
Received in revised form
15 August 2008
Accepted 6 September 2008
Available online 23 September 2008

Keywords:
Apatite
Fluorapatite
Computer simulation
Point defects

ABSTRACT

Atomic scale local density functional simulations and configurational averaging are used to predict the energies and lattice parameters associated with mixed calcium/strontium fluorapatites, $Ca_xSr_{10-x}(PO_4)_6F_2$. In particular, the partition of Sr^{2+} and Ca^{2+} ions between the 6*h* and 4*f* cation sites is established across the entire compositional range. Lattice parameters and lattice volume are also analyzed as a function of Ca^{2+} to Sr^{2+} concentration and their cation site distribution. The predicted internal energy of mixing between the end members is used to discuss the available experimental data.

1. Introduction

1.1. Motivation

Apatite or apatitic isomorphs are perhaps best known as the most abundant mineral phase in the bone and teeth of vertebrates [1]. As a consequence, they are used to replace and repair bone [2]. They are, however, also of industrial importance, finding applications in a range of areas including, for example, catalysis [3]. Furthermore, apatite is the most abundant phosphate mineral [4], being commonly found in igneous rocks, where the fluorapatite variant is generally dominant, but it is also observed in some sedimentary and metamorphic rocks [5]. Given its stability as a natural mineral, apatite is considered a promising candidate for radioactive waste immobilization [6].

For all the cases described above, cation substitutions take place. With waste-form applications in particular, it is clearly important to understand where the various foreign cation species are accommodated in the lattice. In this regard, calcium hydroxyapatite has been synthesized with cadmium substituted for calcium [7], uranium has been accommodated in oxy-silicophosphates [8], lead can be incorporated in calcium fluoro-vanadinite [9], with both strontium and lead being substituted together to form a strontium-lead fluorapatite solid solution [10]. Here atomic scale modelling techniques will be used to predict: the energies associated with Sr^{2+} accommodation in Ca fluorapatite, Ca^{2+} accommodation in Sr fluorapatite and the variation in lattice parameter as a function of the Ca to Sr ratio across the entire $Ca_xSr_{10-x}(PO_4)_6F_2$ solid solution.

1.2. Description of structure

The naturally occurring mineral apatite has the general formula $M_{10}(XO_4)_6A_2$ [4]. The most common anionic groups, A^-, found in phosphate apatites are: F^-, OH^- or Cl^-. In this study we are concerned with the isomorph, fluorapatite, $Ca_5(PO_4)_3F$, which is shown in Fig. 1. Fluorapatite is hexagonal, and exhibits space-group $P6_3/m$ [1,11]. Experimental lattice parameters for $Ca_5(PO_4)_3F$ are: $a = 9.375$ Å and $c = 6.887$ Å [12].

Fluorapatite consists of regular phosphate tetrahedra around two symmetry distinct cation sites: 4*f* and 6*h*. The 4*f*:6*h* ratio is therefore 2:3. The 4*f* site is 9-fold coordinated by oxygen ions, with six shorter Ca–O distances and three longer Ca–O distances. The 6*h* site is 7-fold coordinated, with 6 Ca–O bonds from oxygen atoms associated with phosphate groups and one Ca–F bond with a fluorine anion located in *c*-axis channels (see Fig. 1). The fluorine ions are located at 2*a* sites within the centres of triangles composed of 6*h* cations. A single unit cell contains two formula units i.e. $Ca_{10}(PO_4)_6F_2$.

A useful polyhedron can be described by the six closest O^{2-} ions surrounding the 4*f* site. This metaprism, initially described by White et al. [11], distorts or twists as the chemistry of the apatite changes. The amount of twist is controlled by the

* Corresponding author.
E-mail address: r.grimes@ic.ac.uk (R.W. Grimes).

0022-4596/$ - see front matter © 2008 Elsevier Inc. All rights reserved.
doi:10.1016/j.jssc.2008.09.004

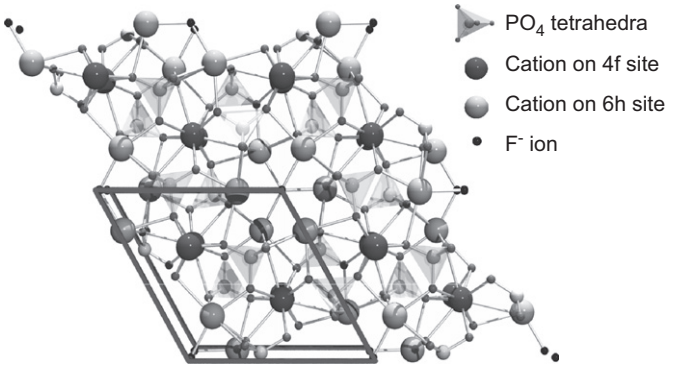

Fig. 1. The fluorapatite ($Ca_{10}(PO_4)_6F_2$) crystal structure viewed along [0001]. The hexagonal primitive unit cell is highlighted by a bold parallelogram, the different ions are described in the key.

relative sizes of ions in the c-axis channel. Dong et al. [13] developed a useful model relating the lattice parameters to the metaprism twist angle.

1.3. Previous studies concerning Ca^{2+}/Sr^{2+} distributions

A range of previous experimental work has addressed the distribution of Sr^{2+} cations between the 4*f* and 6*h* sites [14–25]. Determination of apatite crystal chemistry from literature data can, however, be problematic for several reasons.

Firstly, discrepancies between chemical analysis and refined occupancies are indicative that the composition or relative stoichiometry of apatite is not always easily determined. This is evident, for example, in previous work by Wilson et al. [14], concerning calcium deficient hydroxyapatites, where NMR and IR spectroscopy show HCO_2^- ions present in the apatite that were not interpreted in the XRD analysis. Also, Dong et al. [13], found in calcium-lead fluoro-vanadinite apatite a reduction in crystallinity for some compositions and a secondary phase of $Ca_3(VO_4)_2$. Misinterpretation could therefore occur if the composition is not independently verified. In single crystal studies this potential source of error is obviously less significant than where powder analysis, such as Rietveld [26], has been undertaken. In other words, if full structure refinement is not undertaken the distribution of ions on the different crystallographic sites cannot necessarily be guaranteed.

Secondly, for full cation order to become apparent, the structure could require a significantly longer annealing time than typically allowed for the general structure to equilibrate. Dong et al. [9] have shown that several weeks were necessary to stabilize the distribution of cations over the two sites in calcium-lead fluoro-vanadinite apatite.

Investigating mixed calcium-strontium fluorapatites crystallized from a glass composition of $4.5SiO_23Al_2O_31.5P_2O_53CaO2CaF_2$, Hill et al. [16] ascertained through a combination of MAS-NMR, Differential Thermal Analysis, X-ray powder diffraction and neutron diffraction, that 6*h* sites are more likely to be occupied by Ca^{2+} than Sr^{2+}. It was proposed that this is due to the higher charge size ratio of Ca^{2+} relative to Sr^{2+}, giving Ca^{2+} a greater affinity with the F^- anion.

Hughes et al. [15] argue that bond valance sums for Ca^{2+} and Sr^{2+} in apatite explain the X-ray diffraction data concerning two compositions of Ca apatite containing 29% and 63% Sr^{2+} respectively, for which the majority of Sr^{2+} was found at 6*h*. It was suggested that Sr^{2+} is over bonded at both sites but less-so at 6*h*, concluding that Sr^{2+} would preferentially order at the 6*h* site. These findings were later supported by Rakovan et al. [17]. Conversely, Heijligers et al. [18] and Andrés-Vergés et al. [19], using powder X-ray and IR spectra respectively, concluded that Sr^{2+} occupies both sites but the 4*f*: 6*h* ratio for Sr^{2+} varies as a function of composition.

Lastly, Khattech and Jemal [27] have determined the standard enthalpy of formation and the enthalpy of mixing of Ca apatite with Sr apatite. The enthalpy of mixing as a function of Sr to Ca ratio showed a distinct maximum at approximately 60% Sr. This was attributed to the preferential substitution of Sr^{2+} at the (larger) 6*h* site (i.e. reflecting the site ratio).

Studies of related apatites also suggest a complex distribution of cations. For example, Sudarsanan et al. [20,21] carried out XRD analysis on mixed $Ca_xSr_{10-x}(PO_4)_6Cl_2$ finding, at low concentrations of Sr^{2+}, a preference for substitution at 6*h*, however this preference decreased with increasing Sr^{2+} content. Khndolozhin et al. [22] who considered Sr^{2+} substituted calcium-hydroxyapatite, found that 6*h* sites are preferentially filled up to ~10% Sr^{2+}, with the degree of order decreasing as the percentage of Sr^{2+} increased. Another study of Sr^{2+} substituted calcium-hydroxyapatite by Kikuchi et al. [23] suggested that Sr^{2+} substitution occurs preferentially at the 4f site. However, the opposite conclusion was made by Bigi et al. [24] who again determined a preference for Sr^{2+} substitution at the 6*h* site. Recently Bigi et al. [25] extended their original work and provided a more complete picture for Sr^{2+} site preference. In particular the found a very slight preference for Sr^{2+} occupation of the 4*f* site in crystals containing 1.9% Sr, but in samples containing more than 10% Sr, there was a preference for the 6*h* site.

Lead-strontium fluorapatites were investigated by Badraoui et al. [10] using a combination of X-ray powder diffraction, infra red (IR) analysis and absorption spectophotometry. Reitveld refinement of the occupation factors of Pb^{2+} and Sr^{2+} indicate Sr^{2+} at both sites but with a preference for 4*f*. As Sr^{2+} content increased, the "*a*" lattice parameter decreased, as did the proportion of Sr^{2+} on the 6*h* site. This followed a similar investigation of lead–strontium hydroxyapatites, where it was found that Pb^{2+} preferentially occupied 6*h* [28]. Given the similarity in radii of the two cations, the distribution of the ions over the two sites was attributed to the relative high electronegativity of Pb^{2+}, which increases the polarization of the O–H bond.

Despite the number of previous studies that have addressed the ordering of cations in the apatite structure, conclusions concerning the site preference of Sr^{2+} in Ca fluorapatite are not entirely consistent. As discussed, reasons why this may have occurred include the necessity for extended cation equilibration times [9,13], and minor second phase formation [14]. In this study atomic scale density functional approximation (DFT) simulations will be used to predict internal energy differences for the accommodation of Sr^{2+} at 4*f* and 6*h* sites.

Numerous studies based on a computational approach to studying apatites. In particular, Rabone and de Leeuw studied Sr^{2+} substitution into Ca fluorapatite and Ca hydroxyapatite using classical potentials [29]. Other studies focus on the position and orientation of the common anionic groups along the c-axis channel in apatites. For example, de Leeuw et al., considered aspects such as the local ordering of hydroxyl groups and fluoride ions in hydroxyapatite [30], solid solutions of fluoro-chlorapatites [31] and carbonate defects in hydroxyapatite [32]. Additionally, DFT-Local Density Approximation (LDA) studies of the stoichiometric structures of oxyapatite, hydroxyapatite, fluorapatite, and chlorapatite have been carried out by both Calderin et al. [33] and Rulis et al. [34] who show agreement with experimentally derived structural parameters. Finally, Mercier et al. [35] compared crystal-chemical parameters calculated using DFT-Generalized Gradient Approximation (GGA) with single crystal refinements of a range of different apatite compositions. These

previous studies establish atomic scale simulation as useful and reliable for the study of apatites.

2. Method

2.1. Atomic scale simulations

Following the work by Mercier et al. [35], we choose to employ quantum mechanically based simulations. The present density functional simulations (DFT) employed the plane wave code CASTEP v.4.01 [36] (built using version 9.1 of Intel compilers for a 64 bit × 86 Architecture). Calculations were carried out on a unit cell consisting of 42 ions, under constant pressure conditions. Consequently both unit cell and atomic position parameters were allowed to vary allowing cell volumes to be calculated as a function of composition. The system was modelled at the GGA level of approximation using the PBE (Perdew et al. [37]) functional, ultrasoft pseudopotentials [38,39] and a 540 eV plane wave cut-off (following a study of convergence). The Brillouin zone was sampled on a $2\times2\times3$ Monkhorst-Pack grid [40]. The energy convergence tolerance was 2×10^{-5} eV/ion, and the electrical energy convergence tolerance of the SCF (self consistant field) cycles was 1×10^{-6} eV/ion.

2.2. Selection of configurations

A full geometry optimization of a single unit cell of apatite was carried out, where one Ca^{2+} ion located at the 4*f* site was replaced with a Sr^{2+}, corresponding to a composition of $Ca_9Sr(PO_4)_6F_2$. This was repeated but now replacing a 6*h* Ca^{2+} ion. Similarly for $Sr_9Ca(PO_4)_6F_2$, one 4*f* ion was replaced with a Ca^{2+} and subsequently a 6*h* ion was replaced by a Ca^{2+} ion. In each case, given the "defect" concentration of 10% and a single unit cell, there is only one possible cation distribution (configuration) in each case.

Where there is more than one substitution in the unit cell, the number of possible configurations increases dramatically. For 20% Sr^{2+} in a single cell, (i.e. $Ca_8Sr_2(PO_4)_6F_2$), the two Sr^{2+} ions can be accommodated on either 4*f* or 6*h* sites exclusively, or one on each site. However, given that there are four, 4*f* and six, 6*h* sites there are a number of ways in which the two Sr^{2+} ions can be accommodated even if both are, for example, on 4*f* sites. The total number of symmetry distinct configurations for $Ca_8Sr_2(PO_4)_6F_2$ is 24. At this concentration of 20% Sr^{2+} all 24 configurations were calculated and categorized as either "4*f*", "6*h*" or "mixed". Of course, $Sr_8Ca_2(PO_4)_6F_2$ also has 24 symmetry distinct configurations. Therefore at 80% Sr^{2+} all 24 configurations were calculated and again categorized as "4*f*", "6*h*" or "mixed".

Calculations were also carried out at 30%, 40%, 50%, 60% and 70%. In each case all possible symmetry distinct configurations were identified and calculated: at 30% and 70% 63 configurations, at 40% and 60% 121 configurations and at 50% 149 configurations.

2.3. Configurationally averaged property values

Given the large number of configurations calculated, it is useful to generate property values that are a statistical thermodynamic average over the configurations at each composition [41,42]. If configuration *i* has property value P_i (here these will include lattice parameters, unit cell volumes and lattice energy), then the configurational average is given by,

$$P_i = \frac{\sum_i n_i P_i e^{-\Delta E_i/kT}}{\sum_i n_i e^{-\Delta E_i/kT}} \quad (1)$$

where ΔE_i is the difference between the energy of configuration *i* and the energy of the most stable configuration, *k* is Boltzmann's constant, *T* is the temperature over which the average is taken (here *T* 873 K [43]) and n_i is the number of configurations with the same symmetry that can be generated in the unit cell.

3. Results and discussion

3.1. Lattice volumes

The simulations predict lattice volumes, lattice parameters and lattice energies of unit cells that represent solid solutions between $Ca_{10}(PO_4)_6F_2$ and $Sr_{10}(PO_4)_6F_2$ with composition $Ca_{10-x}Sr_x(PO_4)_6F_2$ where $0\leqslant x\leqslant1$. Fig. 2 shows lattice volumes (configurationally averaged) and compares these to available experimental data [11,15,17,44,45] Although the values predicted are a little higher than experiment, they are consistently higher so that the increase in lattice volume with increasing Sr content (i.e. *x* value) is very well reproduced (as evidenced by the slopes: see Fig. 2). Furthermore, it is apparent that the lattice volumes of the solid solution members fall on an essentially straight line between the two end member compositions. Thus, there is no excess lattice volume associated with solid solution formation.

3.2. Internal energy of mixing

The configurationally averaged solid solution lattice energies are used to predict the internal energy to form the solid solution (i.e. ΔE_{sol}, the excess energy) from the end member compositions according to the expression;

$$\Delta E_{sol} = \Delta E(Ca_{10-x}Sr_x(PO_4)_6F_2) - \left\{\frac{10-x}{10}\right\}\Delta E (Ca_{10}(PO_4)F_2) - \left\{\frac{x}{10}\right\}\Delta E(Sr_{10}(PO_4)_6F_2 \quad (2)$$

where for example, $\Delta E(Ca_{10}(PO_4)_6F_2)$ is the lattice energy of the calcium fluorapatite end member. Fig. 3 shows these calculated internal excess energies of formation as a function of *x* (for both individual configurations and configurationally averaged values) and compares them to the experimental excess enthalpy of formation data of Khattech and Jemal [27] (as did Rabone and de

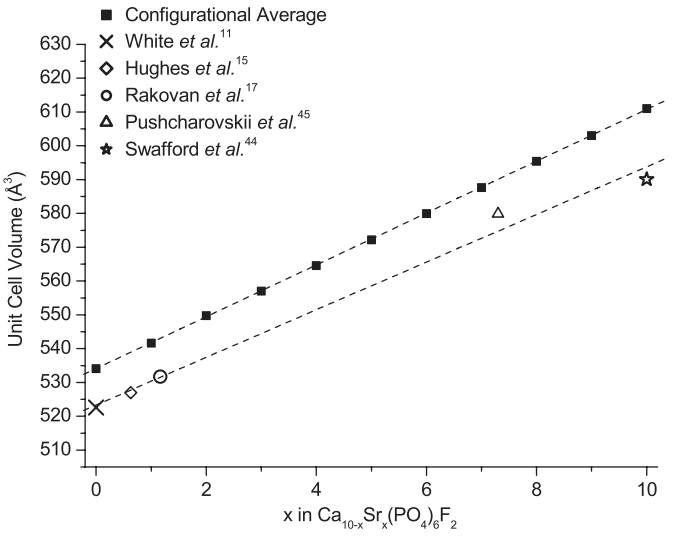

Fig. 2. The unit cell volume of $Ca_{10-x}Sr_x(PO_4)_6F_2$ as a function of *x*. The gradient of the line through the experimental values is 0.71 Å^3/*x* and that through the calculated values is 0.77 Å^3/*x*. The black squares were calculated for this study, all other points are experimental, taken from the literature.

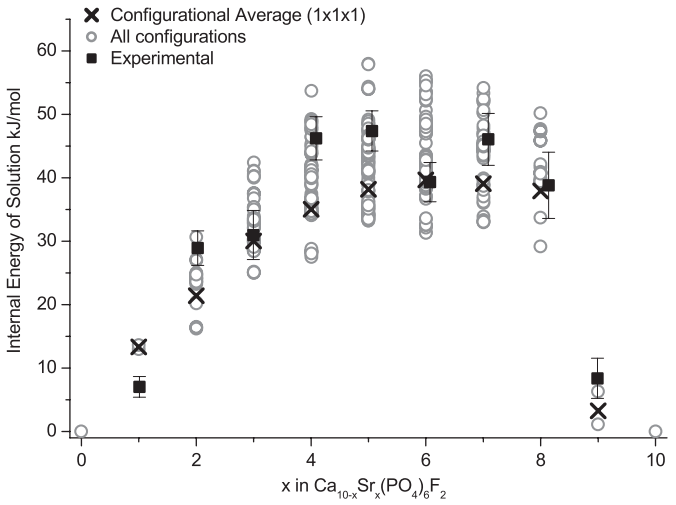

Fig. 3. Comparison of calculated internal energy of solution with experimental enthalpy of solution values (Khattech and Jemal [27]) as a function of Sr^{2+} concentration, defined by x in $Ca_{10-x}Sr_x(PO_4)_6F_2$. All possible configurations, that are possible within a single unit cell, were calculated and configurationally averaged values generated.

Leeuw [29]). Strictly, in order to compare the calculated internal solid solution formation energies with enthalpies, the change in pressure volume term (PV) also needs to be calculated. Fortunately, in this case the change in the PV term is negligible as the excess lattice volume upon solid solution formation is almost zero (as shown by Fig. 2). A second approximation is that the internal energies were calculated at zero temperature whereas the experimental enthalpies were determined at a finite temperature of 298 K. Although some change in enthalpy is expected as a function of temperature, again the fact that we are considering differences in enthalpy means the influence of temperature should be small.

Considering the detailed predicted variation in internal energy of solution (configurationally averaged results, depicted as crosses) across the solid solution (in Fig. 3), it is apparent that it has generated an asymmetric curve, peaking close to a concentration of 60% Sr^{2+} (recall that the 4*f*:6*h* site ratio is 60:40). Furthermore, predicted values at 30%, 60% and 80% match previous experimental results [27] very closely. However, although experimental results also describe an asymmetrical solution enthalpy curve it has an obvious deviation at 60%, where the peak maximum, might be expected. The DFT simulations, however, do not predict such a local deviation from the energy maximum. There are two possibilities. It may be that, the experimental values at 40%, 50% and 70% may be a little high so that the value reported at 60% (which agrees with the DFT prediction) is correct. Alternatively, it is the experimental data point at 60% may not correspond to a single solid solution but to a two phase mixture. That is, a miscibility gap may be opening up around 60% Sr content. Clearly further experimental work is necessary to investigate this possibility further.

Now consider the specific concentrations that relate to 10% Sr content i.e. $Ca_9Sr(PO_4)_6F_2$ and 90% Sr content i.e. $CaSr_9(PO_4)_6F_2$. First, at 10% the difference in excess internal energy of solution between the two possible configurations is 0.007 eV: this is the energy to swap the Sr^{2+} ion between 4*f* and 6*h* sites. It indicates that there is negligible preference for substituting on either site (by negligible we mean the energy difference is considerably less than the configurational entropy of mixing at typical synthesis temperatures (873 K [43]) where for a single unit cell this energy would be ~0.188 eV). For $Sr_9Ca(PO_4)_6F_2$ the difference in energy between substituting Ca^{2+} on 4*f* to substitution on 6*h* is 0.054 eV. Although this energy difference is much larger than for $Ca_9Sr(PO_4)_6F_2$, it is still not large enough to result in a strong preference to occupy either site. The configurationally averaged values for the proportion of 6*h* sites occupied by Sr^{2+} (the occupancies) are 0.581 at the 10% concentration ($x = 1$) and 5.562 at 90% concentration ($x = 9$). Two configurations is clearly a rather small number for such an analysis but at such a low concentration, the minority cations (i.e. Sr^{2+} at $x = 1$ or Ca^{2+} at $x = 9$) will be well separated and as such these two configurations are representative.

Table 1
The internal energy of solution, ΔE_{sol}, for all possible configurations of $Ca_8Sr_2(PO_4)_6F_2$

Percentage of 6*h* sites that are occupied by Sr^{2+}	Percentage of 4*f* sites that are occupied by Sr^{2+}	No. of each configuration possible (n)	ΔE_{sol} (kJ mol^{-1})
0.00	50.00	2	30.71
33.33	0.00	2	27.10
33.33	0.00	2	26.96
33.33	0.00	2	25.05
33.33	0.00	2	24.84
33.33	0.00	1	24.78
33.33	0.00	2	24.78
16.67	25.00	2	24.58
16.67	25.00	2	24.35
16.67	25.00	2	24.20
16.67	25.00	2	24.15
16.67	25.00	1	24.13
16.67	25.00	2	24.08
16.67	25.00	1	24.03
16.67	25.00	2	23.73
16.67	25.00	2	23.68
16.67	25.00	2	23.61
16.67	25.00	2	23.57
16.67	25.00	2	23.26
0.00	50.00	2	20.42
0.00	50.00	2	20.20
33.33	0.00	2	16.53
33.33	0.00	2	16.45
33.33	0.00	2	16.23
Configurationally averaged no. of Sr^{2+} at each site (873 K)			
	6*h*	4*f*	
$Ca_8Sr_2(PO_4)_6F_2$	1.34	0.66	

Table 1 reports the internal energies of solution corresponding to all 24 possible configurations of $Ca_8Sr_2(PO_4)_6F_2$. These volumes are also reported on Fig. 3, depicted as open circles. The configuration with the lowest internal energy (i.e. the most stable) has both Sr^{2+} ions located on 6*h* sites: this corresponds to a 6*h* site occupancy of 0.33. The configurationally averaged number of Sr^{2+} ions occupying 6*h* sites (see Table 1) is 1.32 (the remaining 0.68 occupy 4*f* sites): this corresponds to an occupancy of 0.22. Both the lowest energy configuration and configurational average occupancy values, at this Sr concentration, are reported in Fig. 4. Clearly configurational averaging can yield a significantly different occupancy number than does simply assuming the configuration with the lowest energy or taking a simple mean. Significant differences between the lowest energy configuration and the averaged configuration has been identified in other systems [42,46].

The preference for 6*h* sites to be occupied by Sr^{2+} ions is increasingly evident as the Sr content increases. For $Ca_7Sr_3(PO_4)_6F_2$, the configurationally averaged number of Sr^{2+} ions occupying 6*h* sites is calculated to be 1.78 so that the occupancy is now 0.30. However, the configuration with the lowest energy is that in which two 6*h* sites are occupied by Sr^{2+} ions, with the third Sr^{2+} ion occupying a 4*f* site (this is the open circle with lowest

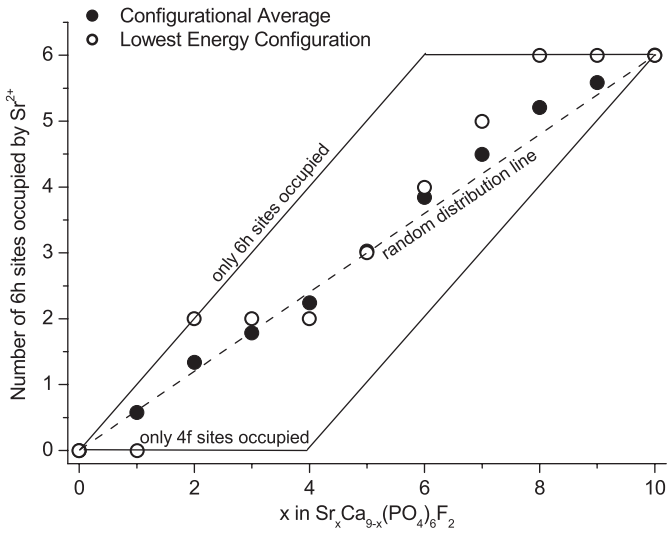

Fig. 4. Occupancy of 6*h* sites by Sr^{2+} ions as a function of composition (x in $Ca_{10-x}Sr_x(PO_4)_6F_2$).

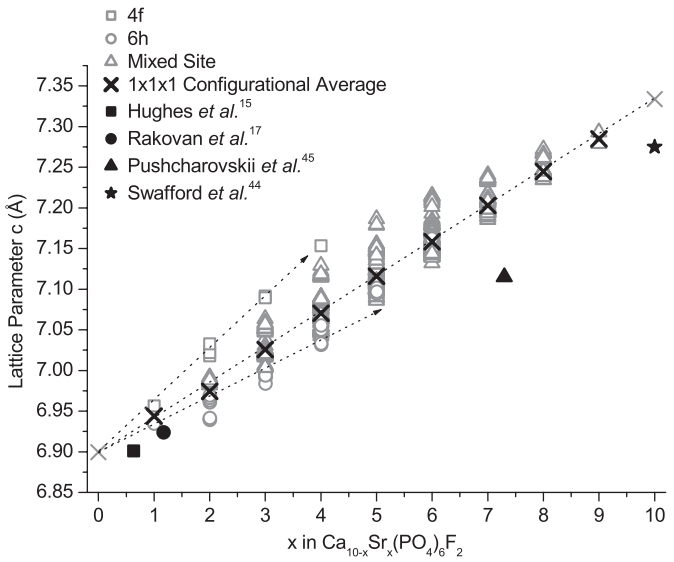

Fig. 5. Change in the "*c*" lattice parameter as function of Sr^{2+} concentration, defined by x in $Ca_{10-x}Sr_x(PO_4)_6F_2$.

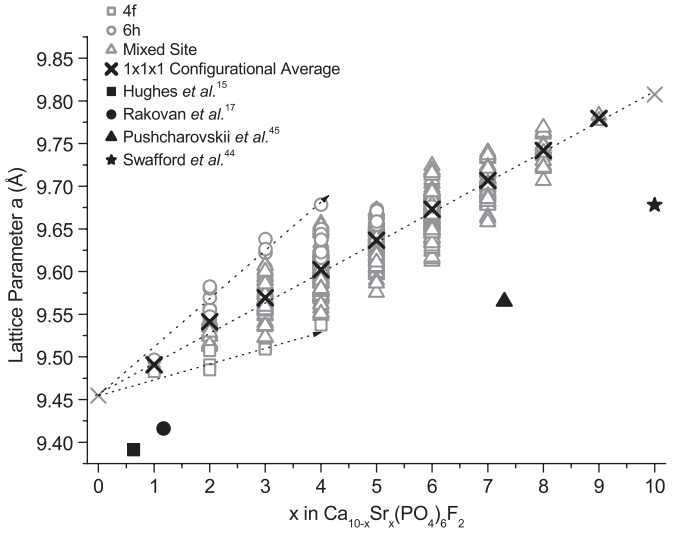

Fig. 6. Change in the "*a*" lattice parameter as a function of Sr^{2+} concentration, defined by x in $Ca_{10-x}Sr_x(PO_4)_6F_2$.

energy at 30% Sr^{2+} shown in Fig. 3). In this case, therefore, configurational averaging yields a rather similar occupancy value to that of the lowest energy configuration.

Results for all other compositions are shown in Fig. 3. The averaged occupancy values, along with the others described above, are reported as a function of composition (x in $Ca_{10-x}Sr_x(PO_4)_6F_2$) in Fig. 4. The graph also shows the number of Sr^{2+} ions on 6*h* sites of the lowest energy configuration at each Sr concentration value investigated (corresponding to the lowest open circles in Fig. 3). Furthermore, the graph displays a dashed line that assumes a completely random distribution of Sr^{2+} ions across 6*h* and 4*f* sites (i.e. a straight line between the end points). This shows that, at 10% Sr^{2+} ion concentration the distribution is very close to the fully random distribution with only a slight preference for more Sr^{2+} ions towards 6*h* sites. However, because there are more 6*h* sites than 4*f* sites, this means that more Sr^{2+} ions occupy 6*h* sites than 4*f* sites. The lack of strong preference for a specific Sr^{2+} ion to occupy a 6*h* site rather than a 4*f* site is therefore in agreement with the experimental observation that Sr^{2+} ions are more likely to be observed at 6*h* sites in fluorapatite [15–17,27], but also in the chloroapatite [20,21] and hydroxyapatite analogues [24,25]. At higher Sr^{2+} concentrations there is a stronger preference for a given Sr^{2+} ion to occupy a 6*h* site and so the predictions at 70–90% Sr concentration are further above the random distribution line. Consequently, there will be an even greater propensity for Sr^{2+} ions to occupy 6*h* sites.

Of course, there are only certain occupancy values that are possible at a given Sr concentration. Finally, therefore, Fig. 4 also shows the envelope of possible occupancy values: the upper boundary corresponding to when Sr^{2+} ions occupy only 6*h* sites until all six are filled, the lower boundary a complete preference for Sr^{2+} ions to initially occupy only 4*f* sites until all four are filled.

3.3. Influence of cation configuration on lattice parameters

As discussed previously, it can be difficult to unambiguously assign cation distributions through the analysis of diffraction data. In much the same way, given the relatively restricted number of cation configurations (in a single unit cell) and the small energy differences between them, predicting cation distributions from internal energies is also challenging. Consequently, we have analyzed the changes in "*a*" and "*c*" lattice parameters as a function of increasing Sr^{2+} content as such data may be more routinely measured experimentally.

Fig. 5 shows the variation of the *c* lattice parameter with Sr^{2+} content and Fig. 6 details results for *a*. Both figures focus on how differently the lattice parameters change if Sr^{2+} content is confined to either 4*f* or 6*h* sites. For example, Fig. 5 shows that initially occupying 4*f* sites leads to a greater increase in the *c* lattice parameter than if 6*h* is exclusively occupied. Of course, once the percentage of Sr^{2+} proceeds beyond 40%, even if 4*f* sites were exclusively occupied by Sr^{2+}, the available 4*f* sites would be filled and it is inevitable that 6*h* sites begin to be occupied. Consequently, the rate of increase decreases. Equivalently, if 6*h* sites are initially exclusively occupied, beyond 60% 4*f* sites must become occupied. Of course, the two regimes eventually meet at 100% Sr^{2+}. This defines an envelope of possible lattice parameter values.

The change in "*a*" lattice parameter with Sr^{2+} occupation of 4*f* vs. 6*h* sites is opposite to that predicted for the "*c*" lattice parameter (Fig. 5), as illustrated in Fig. 6. That is, up to approximately 40% Sr^{2+} occupation of 6*h* distorts the "*a*" lattice parameter more greatly than does occupation of 4*f*. Incredibly, these non-linear differences in a and *c* lattice parameter with configuration cancel almost entirely to yield a volume dependence that is not only independent of configuration but a linear function of Sr^{2+} ion content (see Fig. 2).

Differences in lattice parameters assuming, initially exclusive 6*h* or exclusive 4*f* occupation are sufficiently great that they could be observed experimentally. However, the distribution of Sr^{2+} ions over the two sites, predicted using configurational averaging are close to a random distribution and consequently we predict that, in practice, a close to linear change in "*a*" and "*c*" lattice parameter will be observed. This is shown in Figs. 5 and 6 as configurational averages. Significantly, a linear relationship was found by Bigi et al. [25] for calcium/strontium hydroxyapatites. Thus, one way to test the present predicted site occupation model would be to search for deviations from linear change in the "*a*" and "*c*" lattice parameters as a function of strontium content.

Finally, preference for Sr^{2+} ions to occupy 6*h* sites has previously been ascribed to the idea that the 4*f* is geometrically smaller than 6*h* [1,47] and that the Sr^{2+} ion is larger than Ca^{2+} [48]. However, the present prediction that the increase in volume due to Sr^{2+} ion accommodation is identical for both sites is not consistent with such a view. In fact, it is probably the change in coordination from 6*h* to 4*f* that compensates for any difference in volume between the sites, so that the strains due to Sr^{2+} ions at 6*h* and 4*f* sites are essentially the same. Similarly, discussions of bond valance sums for Ca^{2+} ions [47] suggest the values are 2.17 and 2.08 for 4*f* and 6*h* respectively, showing that the sites are "over bonded" (a term commonly used to indicate that the bond valance sum is greater than the formal charge of the ion [49]), 6*h* less so than 4*f*. Being a larger ion, Sr^{2+} ions on these sites would be even more over bonded with 4*f* and 6*h* bond valance sum of 3.14 and 3.07 respectively. This was a reason previously given for the preferential substitution of Sr^{2+} ions at 6*h* sites [15]. Comparing, however, the bond valance sums for 4*f* and 6*h* sites in the $Ca_9Sr(PO_4)_6F_2$, where the ions surrounding 6*h* and 4*f* sites occupied by Sr^{2+} ions have been allowed to relax to zero force (i.e. using the present predicted values), the difference between the sums becomes negligible; the values for 4*f* and 6*h* being 2.87 and 2.88 respectively (which are, of course, consistent with there being little site preference at this Sr^{2+} concentration).

4. Summary

At low Sr^{2+} ion concentrations there is only a slight energetic preference predicted for a Sr^{2+} ion to occupy a 6*h* site rather than a 4*f* site. Consequently the distribution of Sr^{2+} ions over the 6*h* and 4*f* sites approaches a random distribution. Since there are more 6*h* sites than 4*f*, this means that the majority of Sr^{2+} ions occupy 6*h* sites. As the Sr^{2+} ion concentration increases, there is a greater energetic preference for an individual Sr^{2+} ion to occupy a 6*h* rather than a 4*f* site and this translates into a greater overall preference for Sr^{2+} ions to be observed at 6*h* sites. This preference for Sr^{2+} ions to be located at 6*h* sites is in agreement with the majority of experimental studies [15–17,20,21,24,25,27]. The calculated internal energies for solution predicts an asymmetric curve across the compositional spectrum, similar to that observed experimentally [26] but without agreement at every composition.

We predict that a strong preference for Sr^{2+} ions to occupy 6*h* sites, will result in a nonlinear increase in the "*a*" lattice parameter but an opposite nonlinear increase in the "*c*" lattice parameter. Consequently there is an overall linear increase in volume upon Sr^{2+} substitution irrespective of the Sr^{2+} ion distribution. However, the predicted configurational average occupation values leads to a distribution of Sr^{2+} ions over 6*h* and 4*f* sites which is sufficiently close to random that an essentially linear change in lattice parameters is expected.

Acknowledgements

We wish to thank Tim White, Nick Ashley, Jon Ball and David Parfitt for valuable discussions. This work was carried out as part of the TSEC programme KNOO and as such we are grateful to the EPSRC for funding under grant EP/C549465/1. EMM acknowledges AWE for additional financial support. Computing resources were provided by the Imperial College High Performance Computing Service, URL: http://www.imperial.ac.uk/ict/services/teachingandresearchservices/highperformancecomputing.

References

[1] D. McConnell, Apatite, Its Crystal Chemistry, Mineralogy, Utilization, and Geologic and Biologic Occurances, Springer, Wien, 1973.
[2] Z.Y. Li, W.M. Lam, C. Yang, B. Xu, G.X. Ni, S.A. Abbah, K.M.C. Cheung, K.D.K. Luk, W.W. Lu, Biomaterials 28 (7) (2007) 1452–1460.
[3] S. Sugiyama, Journal of Materials Chemistry 6 (3) (1996) 459–464.
[4] J.O. Nriagu, P.B. Moore, Phosphate Minerals, Springer, Berlin, New York, 1984.
[5] W.A. Deer, R.A. Howie, J. Zussman, An Introduction to the Rock-Forming Minerals, Longman Scientific & Technical, 1993.
[6] I.W. Donald, Journal of Materials Science 32 (22) (1997) 5851–5887.
[7] M. Srinivasan, C. Ferraris, T. White, Environmental Science & Technology 40 (22) (2006) 7054–7059.
[8] R. El Ouenzerfi, M.-T. Cohen-Adad, C. Goutaudier, G. Panczer, Solid State Ionics 176 (1–2) (2005) 225–231.
[9] Z. Dong, T.J. White, Acta Crystallographica Section B 60 (2) (2004) 138–145.
[10] B. Badraoui, A. Aissa, A. Bigi, M. Debbabi, M. Gazzano, Journal of Solid State Chemistry 179 (10) (2006) 3065–3072.
[11] T.J. White, D. ZhiLi, Acta Crystallographica Section B 59 (1) (2003) 1–16.
[12] P. Comodi, Y. Liu, P.F. Zanazzi, M. Montagnoli, Physics and Chemistry of Minerals 28 (4) (2001) 219–224.
[13] Z. Dong, T.J. White, Acta Crystallographica Section B 60 (2) (2004) 146–154.
[14] R.M. Wilson, J.C. Elliott, S.E.P. Dowker, Journal of Solid State Chemistry 174 (1) (2003) 132–140.
[15] J.M. Hughes, M. Cameron, K.D. Crowley, American Mineralogist 76 (11–12) (1991) 1857–1862.
[16] R.G. Hill, A. Stamboulis, R.V. Law, A. Clifford, M.R. Towler, C. Crowley, Journal of Non-Crystalline Solids 336 (3) (2004) 223–229.
[17] J.F. Rakovan, J.M. Hughes, Canadian Mineralogist 38 (2000) 839–845.
[18] H.J.M. Heijligers, R.M.H. Verbeeck, F.C.M. Driessens, Journal of Inorganic & Nuclear Chemistry 41 (5) (1979) 763–764.
[19] M. Andres-Verges, F.J. Higes-Rolandi, P.F. Gonzalez-Diaz, Journal of Solid State Chemistry 33 (1980) 125–126.
[20] K. Sudarsanan, R.A. Young, Acta Crystallographica Section B 30 (6) (1974) 1381–1386.
[21] K. Sudarsanan, R.A. Young, Acta Crystallographica Section B 36 (7) (1980) 1525–1530.
[22] V.O. Khudolozhkin, V.S. Urusov, K.I. Tobelko, Geochemistry International 9 (1972) 827.
[23] M. Kikuchi, A. Yamazaki, R. Otsuka, M. Akao, H. Aoki, Journal of Solid State Chemistry 113 (2) (1994) 373–378.
[24] A. Bigi, G. Falini, M. Gazzano, N. Roveri, E. Tedesco, Materials Science Forum 278-2 (1998) 814–819.
[25] A. Bigi, E. Boanini, C. Capuccini, M. Gazzano, Inorganica Chimica Acta 360 (2007) 1009–1016.
[26] H. Rietveld, Acta Crystallographica 22 (1) (1967) 151–152.
[27] I. Khattech, M. Jemal, Thermochimica Acta 298 (1–2) (1997) 23–30.
[28] B. Badraoui, European Journal of Inorganic Chemistry 1864 (2002) 1870.
[29] J.A.L. Rabone, N.H. de Leeuw, Journal of Computational Chemistry 27 (2006) 253–266.
[30] N.H. de Leeuw, Physical Chemistry Chemical Physics 4 (2002) 3865–3871.
[31] N.H. de Leeuw, Chemistry of Materials 14 (1) (2002) 435–441.
[32] S. Peroos, Z. Du, N.H. de Leeuw, Biomaterials 27 (9) (2006) 2150–2161.
[33] L. Calderín, M.J. Stott, A. Rubio, Physical Review B 67 (13) (2003) 134106.
[34] P. Rulis, L. Ouyang, W.Y. Ching, Physical Review B (Condensed Matter and Materials Physics) 70 (15) (2004) 155104–155108.
[35] P.H.J. Mercier, Acta Crystallographica. Section B, Structural Science 61 (2005) 635–655.
[36] M.D. Segall, P.J.D. Lindan, M.J. Probert, C.J. Pickard, P.J. Hasnip, S.J. Clark, M.C. Payne, Journal of Physics-Condensed Matter 14 (11) (2002) 2717–2744.

[37] J.P. Perdew, K. Burke, M. Ernzerhof, Physical Review Letters 77 (18) (1996) 3865–3868.
[38] I.-H. Lee, R.M. Martin, Physical Review B 56 (12) (1997) 7197.
[39] J.P. Perdew, K. Burke, M. Ernzerhof, Physical Review Letters 78 (7) (1997) 1396.
[40] H.J. Monkhorst, J.D. Pack, Physical Review B 13 (12) (1976) 5188.
[41] N.J. Ashley, Journal of Materials Science 42 (6) (2007) 1884–1889.
[42] I.T. Todorov, N.L. Allan, M.Y. Lavrentiev, C.L. Freeman, C.E. Mohn, J.A. Purton, Journal of Physics: Condensed Matter 16 (27) (2004) S2751.
[43] T. White, S.C. Lim, Personal Communication (2007).
[44] S.H. Swafford, E.M. Holt, Solid State Sciences 4 (6) (2002) 807–812.
[45] D.Y. Pushcharovskii, T.N. Nadezhina, A.P. Khomyakov, Kristallografiya 32 (1987) 891–895.
[46] J.-R. Martinez, C.E. Mohn, S. Stolen, N.L. Allan, Journal of Solid State Chemistry, Corrected Proof, in press.
[47] J.M. Hughes, C. Maryellen, K.W. Crowley, American Mineralogist 74 (1989) 870–876.
[48] R.D. Shannon, Acta Crystallographica Section A 32 (Sep1) (1976) 751–767.
[49] A. Santoro, I. Natali Sora, Q. Huang, Journal of Solid State Chemistry 143 (1) (1999) 69–73.